On the variability of tropospheric gases: Sampling, loss patterns, and lifetime

Nancy A. C. Johnston,[1] Jonah J. Colman,[2] Donald R. Blake,[1] Michael J. Prather,[3] and F. Sherwood Rowland[1]

Received 26 March 2001; revised 26 July 2001; accepted 10 September 2001; published 4 June 2002.

[1] The relationship between the variability (relative standard deviation, σ) in mixing ratio of a gas and its global mean lifetime (τ) has been used to estimate the τ of atmospheric gases. This can prove quite useful if it is a unique relationship. Here a three-dimensional chemical transport model is used to investigate the variability-lifetime relationship of tropospheric gases with two types of sources and three types of losses. The effects of sampling time and location are also explored. The relationship is best described in the form $\sigma = \alpha\tau^{-\beta}$, where α and β are variable depending on the sources, sinks, and time and location of averaging. When spatially averaging over the troposphere and temporally averaging over 1 year, the model results give a β of 0.77–0.79 for τ between 0.9 and 7.0 years. The variability of a CH_3Br-like gas is also analyzed using different weightings of chemical sinks. Photochemical (OH), ocean mixed layer, and soil losses are scaled separately to maintain $\tau \approx 1$ year. These different scalings result in a ±17% spread in σ, which translates into a ±20% spread in τ inferred from the variability-lifetime relationship found in the model. In addition, the model is used to simulate conditions of Pacific Exploratory Mission (PEM) Tropics A and B field campaigns. The variability-lifetime relationships derived from the model do not compare to the field observations, except that both demonstrate a seasonal dependence of variability. This study identifies some factors controlling the variability of trace gases in the troposphere, estimates the error in using variability-lifetime analysis to determine an unknown τ, and shows that the variability-lifetime relation is not universal among trace gases. *INDEX TERMS:* 3210 Mathematical Geophysics: Modeling; 0368 Atmospheric Composition and Structure: Troposphere—constituent transport and chemistry; 0365 Atmospheric Composition and Structure: Troposphere—composition and chemistry; 0312 Atmospheric Composition and Structure: Air/sea constituent fluxes (3339, 4504); *KEYWORDS:* variability, lifetime, troposphere, methyl bromide, modeling, PEM-Tropics A and B

1. Introduction

[2] The large-scale variability of the mixing ratio of an atmospheric trace gas is affected by its sources, sinks, and transport. The global mean atmospheric lifetime (τ) is an integrative measure of the sinks, relating atmospheric loss to atmospheric burden in steady state conditions. Generally, variability is described as the fluctuation of an observed measurement around its mean value, or as the standard deviation, s. When s is normalized to the mean value ($s/\bar{x}$) this is referred to as the relative standard deviation, σ.

[3] Can anything be learned about τ of a gas by simply measuring the variability in its atmospheric mixing ratio experimentally? This question has been pondered since *Junge* [1963] first hypothesized that τ of an atmospheric gas was inversely related to its variability in mixing ratio. *Junge* [1974] later examined this relationship using a two-dimensional (2-D) numerical model for gases with τ between 5 days and 1.5 years and observations of gases with τ ranging from 5 days to 10^7 years. The results were described as $\sigma = 0.0216\tau^{-0.95}$ and $\sigma = 0.14\tau^{-1}$ for the model and observations, respectively, where τ is in years. *Junge* [1974] discussed the occurrence of an inverse variability-lifetime relationship as a result of specific conditions. He considered tropospheric gases with the same sources and fairly uniform sinks. The gases should be well mixed in the troposphere and in steady state. The time period of averaging should be at least 1 year. At about the same time, *Gibbs and Slinn* [1973] used a simple mathematical model to describe concentration fluctuations of exponentially decaying gases as proportional to $\tau^{-0.5}$. This result applied to the sampling of long-range trajectories of air masses at a single location, with fluctuations due only to the removal rate. *Gibbs and Slinn* [1973] discuss the temporal variability of a gas at one point in space over time, whereas *Junge* [1974] discusses the spatial variability of a gas over the global troposphere. Formulations for the relationship between temporal variability and τ were also derived theoretically by *Jaenicke* [1982] and *Slinn* [1988].

[4] Others have also explored the relationship between spatial variability and τ. The results are usually expressed in the form of

$$\sigma = \alpha\tau^{-\beta}, \quad (1)$$

where α and β are constants that depend on the time and spatial distribution of the measurements, sources, and sinks (see Table 1). *Hamrud* [1983] used a 2-D model to examine the spatial variability, with varying results depending on the location of sources, types of sinks, and the measure of variability used. This is perhaps one of the most rigorous modeling studies of variability and τ, using three different source and sink functions. The results ranged from 0.048 to 0.49 for α and from 0.63 to 0.91 for β. *Hamrud* [1983] concluded that the uncertainty in the estimate of τ

[1]Department of Chemistry, University of California, Irvine, Irvine, California, USA.
[2]Los Alamos National Laboratory, Los Alamos, New Mexico, USA.
[3]Department of Earth Systems Science, University of California, Irvine, Irvine, California, USA.

0148-0227/02/2001JD000669$09.00

Table 1. Summary of Variability-Lifetime Relation Values in the Literature[a]

α	β	Species	Type	Source
1	0.5		theory	*Gibbs and Slinn* [1973]
0.0216; 0.14	0.95; 1	$10^{-2} < \tau < 1.5$ years; He, Ar, H_2, O_2 CO_2, N_2O, CH_4, CO, O_3, H_2O	theory; observations	*Junge* [1974]
–	0.5, 1.0	$10^{-5} < \tau < 10^{-1}$ years, $10^{-1} < \tau < 10^{5}$ years	theory	*Jaenicke* [1982]
0.048–0.49	0.63–0.91	$0.05 < \tau < 64$ years	2-D model	*Hamrud* [1983]
0.71, 0.29	0.5, 1.0	$10^{-3} < \tau < 10^{-1}$, $10^{-1} < \tau < 10^{4}$ years	theory	*Slinn* [1988]
–	0.48	$0.3 \times 10^{-3} < \tau < 0.3$ years	3-D model	*Ehhalt et al.* [1998]
1.61–3.04	0.28–0.56	C_2-C_8 Hydrocarbons ($10^{-2} < \tau < 10^{2}$ years)	observations	*Jobson et al.* [1988][b]
0.06	1.32	C_2H_6, $CHCl_3$,CH_3Cl, CH_3Br	observations	*Colman et al.* [1998]
0.17–4.3	0.18–0.97	hydrocarbons, halocarbons ($10^{-2} < \tau < 10^{2}$ years)	observations	*Jobson et al.* [1999][b]
4.63	0.64	hydrocarbons, CO, CH_3OH, CH_3CCN, CH_3CHO, CH_3SCH_3, other organics	observations	*Williams et al.* [2000][b]

[a] With σ equal to $\alpha\tau^{-\beta}$.
[b] Studies based on the standard deviation of the ln (x), where x is the mixing ratio. The value s(ln (x)) approaches σ at small values.

is a factor of 10 or more if only the variability is known, but is decreased to about a factor of 2 if some information on the sources and sinks is known. More recently, the spatial variability relation has been applied to observations of atmospheric gases with τ of ~1 year or less [*Colman et al.*, 1998; *Ehhalt et al.*, 1998]. *Ehhalt et al.* [1998] used a 3-D model to investigate tracers with τ from 1 to 100 days, with the resulting variability being proportional to $\tau^{-0.48}$. They found a similar relationship in the variability of alkanes (measured during NASA's Pacific Exploratory Mission (PEM) West B campaign) with respect to the reaction rate constant with OH. *Colman et al.* [1998] used the empirical spatial variability of compounds measured during NASA's PEM-Tropics A campaign and the τ of these compounds with respect to OH loss to estimate τ of methyl bromide (CH_3Br) as 0.8 ± 0.1 years. Other applications of the variability-lifetime relation include the use of the standard deviation of the natural log of the mixing ratio [s(ln (x)] for a measure of variability for observed gases with τ ranging from days to several hundred years [*Jobson et al.*, 1998, 1999; *Williams et al.*, 2000]. All the works mentioned above illustrate an inverse relationship between variability and τ.

[5] A unique variability-lifetime relationship can be used to derive τ of a gas based solely on its measured variability. This can prove quite useful since τ can give information about the atmospheric fluxes of a gas. The estimate of τ of CH_3Br by *Colman et al.* [1998], for example, can be used to assess the contribution of this gas to stratospheric ozone depletion. How universal is a variability-lifetime relation? What kind of error or uncertainty is associated with making τ estimates using this approach? These questions are addressed using a 3-D chemical transport modeling (CTM) study of variability and τ and trace gas observations from NASA's PEM-Tropics A and B (hereinafter referred to as PTA and PTB, respectively).

[6] The definitions chosen to represent variability and lifetime are now specified. The global mean steady state lifetime from tropospheric loss of each simulated gas is calculated in the CTM from the global budgets by dividing the average integrated global content M (in kilograms) by the integrated tropospheric loss L (in kg yr^{-1}) over 1 year:

$$\tau = \frac{M}{L}. \tag{2}$$

The tropospheric τ incorporates the global distribution of mixing ratios and losses and thus depends on the time and location of emissions. For example, if a tracer gas with a $k_{OH} = 1.45 \times 10^{-11}$ exp (−1550/T), where T is the temperature in kelvins, is emitted from a point source starting in January at 180°W and 60°N, 30°N, 0°, and 30°S, the resulting τ with respect to photochemical loss are 0.98, 0.91, 0.88, and 0.80 years, respectively. When the tracer is emitted uniformly from land areas between 56°S and 72°N during the same time, the resulting τ is 0.90 years. When the tracer is emitted from only industrialized regions, τ is longer (0.93 years) because more tracer accumulates at high latitudes where OH values are smaller. Land and industrial sources are considered in section 4 with respect to the variability-lifetime relationship. The dependence of τ on the pattern of emissions is further discussed by *Olsen et al.* [2000]. For gases measured in PTA and PTB, τ is based on a global mean OH concentration of 9.7×10^5 molecules cm^{-3} [*Prinn et al.*, 1995], an average tropospheric temperature of 277 K [*Prather and Spivakovsky*, 1990], and OH rate constants for each gas [*DeMore et al.*, 1997].

[7] The area-weighted mean and root mean square deviation are calculated by

$$\bar{x_w} = \frac{\sum x_i w}{\sum w} \tag{3}$$

$$S_w = \sqrt{\left| \frac{\sum x_i^2 w}{\sum w} - \left(\frac{\sum x_i w}{\sum w} \right)^2 \right|}, \tag{4}$$

where x_i is the mixing ratio at any given time or location and w is the area of the grid box. The variability is described by

$$\sigma = S_w / \bar{x}_w, \tag{5}$$

and the volume of space and time period of averaging is specified. In section 3, σ is calculated from tracer mixing ratios over 6048 global tropospheric grid boxes (σ_{trop}), and the temporal σ is calculated from tracer mixing ratios at one grid box (σ_{local}), both over the period of 1 year (1095 time steps). Thus σ is both spatially and temporally averaged. Another illustration of spatial and temporal variability is CH_3Br measurements taken over the Pacific Ocean during one 8-hour flight of PTA or PTB.

[8] Here the spatial and temporal variability of trace gases are explored using a 3-D CTM, described in section 2. The objectives

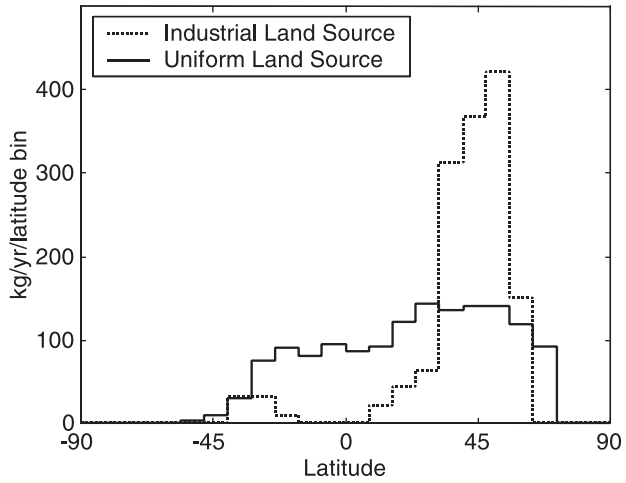

Figure 1. Tracer emissions in kg yr^{-1}/latitude bin for continental land source (solid line) and industrial source (dotted line).

here are similar to *Hamrud*'s [1983] 2-D modeling study, and his results will be compared with the 3-D results of this study. A basic test of the variability-lifetime relation using land-emitted, photochemically reactive tracers is described in section 3. Gases with τ between 0.04 and 7 years are examined by the CTM. Both spatial and temporal variability are discussed in their relation to τ. The variability-lifetime relation is then further developed using different sources and sinks for CH_3Br-like gases in section 4. CH_3Br is specifically selected because it has both industrial and natural sources and several sinks (photochemical, ocean, and soil), and its τ has been previously estimated by *Colman et al.* [1998]. The uncertainty of using a derived relation as above is addressed. In section 5 the model results are compared to atmospheric observations from PTA and PTB. Gases with τ between 0.2 and 1.3 years are selected from those experimentally measured, consistent with *Colman et al.* [1998].

2. Model Description

[9] The University of California (UCI) CTM, adapted from *Prather et al.* [1987], is used to solve the continuity equations for chemical species over a global 3-D grid. A split operator method calculates the separate effects of advection, convection, diffusion, sources, and chemistry. The grid resolution is 8° in latitude and 10° in longitude. The CTM contains nine vertical layers centered at pressure levels of 975, 909, 800, 645, 478, 328, 206, 112, and 40 mbar, with the upper two being stratospheric layers. The Goddard Institute for Space Studies General Circulation Model II supplies the meteorological data and daily wind fields [*Hansen et al.*, 1983]. These data include 8-hour averages of mass flux, pressure fields, convection frequencies, and 5-day averages of temperature. Photochemical loss of tracer by reaction with OH is calculated using a second-order, temperature-dependent rate constant ($k_{OH} = A \exp(-B/T)$) and 5-day average OH concentrations from *Spivakovsky et al.* [1990]. The meteorological and chemical fields are recycled annually in the CTM. The CTM is extensively documented for many tropospheric applications: chlorofluorocarbons [*Prather et al.*, 1987], ^{85}Kr [*Jacob et al.*, 1987], CO_2 [*Fung et al.*, 1987], ^{222}Rn [*Jacob and Prather*, 1990; *Balkanski and Jacob*, 1990], CH_3CCl_3 [*Spivakovsky et al.*, 1990], CH_4 [*Fung et al.*, 1991], ^{210}Pb [*Balkanski et al.*, 1993], and continental O_3 [*Jacob et al.*, 1993a, 1993b].

[10] A separate algorithm is created to generate ocean loss frequencies for a CH_3Br-like gas. These calculations use 1° by 1° latitude by longitude ocean climatology distributed by the National Center for Atmospheric Research (Global Oceanographic Data Set Atlas available from University Corporation for Atmospheric Research at http://www.dss.ucar.edu/datasets/ds279.0), including sea surface temperature, sea surface wind speed, and mixed-layer depth. A net ocean loss frequency is calculated based upon chemical and mixing loss and air-sea exchange as adapted from *Yvon and Butler* [1996]. The resulting loss frequencies are used in section 4 to simulate ocean loss of tracer gases.

[11] In the CTM simulations the tracer is released at a constant emission rate with time using one of two source distributions located in the bottom layer of the grid: a continental land source weighted by land area in grid boxes between 56°S and 72°N latitudes or an industrial source of which 95% lies in the Northern Hemisphere (United States, Europe, Asia, and Japan) (Figure 1). The tracer is subjected to photochemical loss via reaction with OH. The tracer gas mixing ratios are measured in parts per trillion by volume (pptv) and do not affect the OH strength. A soil loss is mimicked by a simple dry deposition velocity loss of tracer weighted by land area in the bottom layer of the grid. Major desert areas (the Sahara in Africa) are omitted in the soil sink. The model is run until annual steady state conditions are achieved, i.e., when the source strength equals the sink strength.

3. Variability and Lifetime Dependence

3.1. Model Simulation

[12] The purpose of these simulations is to test the variability-lifetime relationship for land-emitted gases with a photochemical sink. The resulting spatial variability of eight different tracers is measured by σ (equation (5)) in the CTM. The continental land

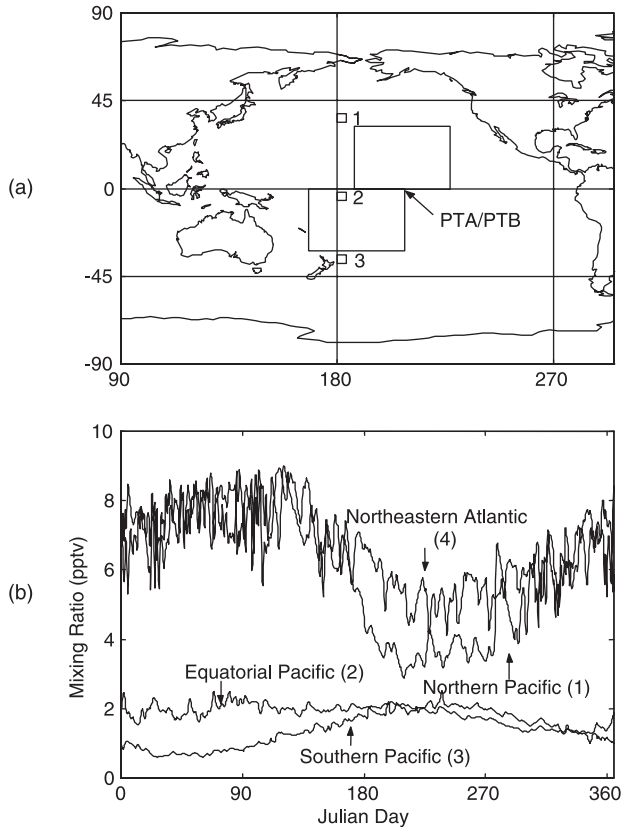

Figure 2. (a) Geographical areas monitored in model simulations. The numbered sites represent one surface grid cell each, and boxed areas represent subsets of PEM-Tropics A and PEM-Tropics B sampling area. (b) Time series of mixing ratio (in parts per trillion by volume (pptv)) of tracer gas (τ = 0.9 years) at four surface locations.

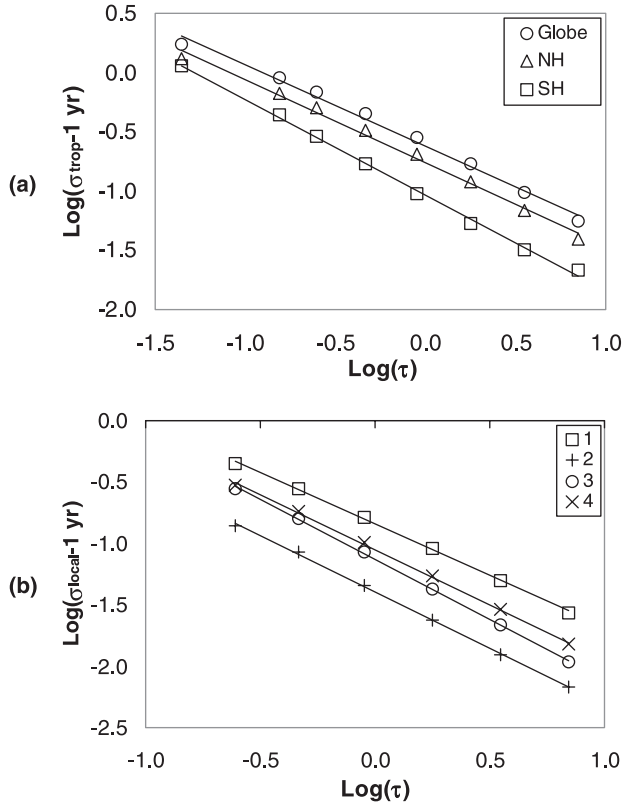

Figure 3. (a) Test of spatial variability-lifetime relation for land-source, photochemical-loss tracers. Results shown include the different volumes sampled: the entire global troposphere (Globe, $\sigma = 0.24\tau^{-0.69}$), and the Northern (NH, $\sigma = 0.17\tau^{-0.70}$) or Southern (SH, $\sigma = 0.09\tau^{-0.81}$) Hemispheric fractions of the troposphere. (b) Temporal variability of six land-source, photochemical-loss tracers at four surface locations: (1) "Northern Pacific" ($\sigma = 0.14\tau^{-0.84}$), (2) "Equatorial Pacific" ($\sigma = 0.04\tau^{-0.92}$), (3) "Southern Pacific" ($\sigma = 0.07\tau^{-0.98}$), and (4) "Northeastern Atlantic" ($\sigma = 0.09\tau^{-0.90}$). All R^2 values are 0.99.

source is used with a constant flux of 1×10^6 g yr^{-1} of tracer gas. The only tropospheric sink is scaled photochemical loss, in which the preexponential factor of k_{OH} is varied to give eight different τ, ranging from 0.04 years (2 weeks) to 7 years. All values of τ refer to the global mean steady state tropospheric lifetime (equation (2)). The 7-year τ tracer ($k_{OH} = 1.82 \times 10^{-12} \exp(-1550/T)$) resembles CH_3CCl_3. The exponential factor (B) is held constant at 1550 K for all other tracers. The tracer mixing ratio is monitored throughout the global grid and at four surface grid boxes over the course of 1 year. The spatial variability is based on tropospheric mixing ratios (σ_{trop}). The calculated σ_{trop} is further distinguished by regions: global, Northern Hemispheric, and Southern Hemispheric troposphere, σ_{GL}, σ_{NH}, and σ_{SH}, respectively. For example, σ_{NH} is calculated using the mixing ratios in all Northern Hemispheric boxes in the troposphere. The temporal variability is calculated using time-evolving mixing ratios at single surface grid boxes. Figure 2a shows three of these locations as well as the area monitored in the CTM for PTA and PTB (section 5). The tracer mixing ratios for one steady state year are shown for all four locations in Figure 2b.

3.2. Results and Discussion

3.2.1. Spatial and temporal variability. [13] The 1-year tropospheric variability (σ_{trop}(1 year)) is plotted against τ in Figure 3a. It is shown that the area of measurements or sampling affects the variability of these gases. The global troposphere causes more variability then either of the two hemispheres alone, while the Southern Hemisphere is less variable than the Northern Hemisphere. The variability in the CTM simulations is most likely caused by the nonuniformity of the land-source distribution (the source is predominantly in the Northern Hemisphere). The values of σ_{GL} are greater than either σ_{NH} or σ_{SH} because of the large latitudinal (north to south) gradient created from the source distribution. The photochemical loss also contributes to the variability of the tracers. However, the seasonal loss fluctuations in each hemisphere are likely to be canceled out when averaging over 1 year.

[14] Power fits to the variability-lifetime relations observed in Figure 3a yield values of α from 0.09 to 0.24 and β from 0.69 to 0.81. The R^2 values are all >0.99 for each of these power fits. These results are comparable to those that *Hamrud* [1983] observed (Table 1). The most applicable experiment from *Hamrud* [1983] is the anthropogenic source combined with the uniform sink ($\sigma = 0.31\tau^{-0.72}$). The variability of the short-lived gases can be compared to the 3-D model results of *Ehhalt et al.* [1998], where β was close to 0.5. Tracers with $0.04 < \tau < 0.5$ years from Figure 3a give β of 0.59 and 0.57 for the Northern Hemisphere and global troposphere, respectively. The area monitored in the *Ehhalt et al.* [1998] study was located in the Northern Hemisphere and was averaged over the month of March. Thus the different time and spatial scales will result in differences in the variability-lifetime relation. *Slinn* [1988] also demonstrated that sampling time affects the variability-lifetime relation. For example, a 1-year sampling time gives higher values of σ than a 1-month sampling time. When the sampling time is much greater than τ, the relationship deviates from *Junge*'s [1974] result (τ^{-1}) and resembles $\tau^{-0.5}$. *Jaenicke* [1982] also pointed this out in his assessment of aerosols using a first-order removal temporal model.

3.2.2. Temporal variability. [15] The temporal variability of six tracers is calculated at the four surface locations (Figure 2b). These sites include (1) "Northern Pacific Ocean," 36°N, 178°W; (2) "Equatorial Pacific Ocean," 4°S, 178°W; (3) "Southern Pacific Ocean,"36°S, 178°W; and (4) "Northeastern Atlantic Ocean" (Ireland), 52°N, 8°W. The resulting σ_{local} (1 year) is shown in Figure 3b. The location with the highest variability is in the northern Pacific Ocean, while the lowest σ is near the equatorial Pacific Ocean. This is likely caused by the concentrated source strength in the Northern Hemisphere, as is further evidenced by the high variability of the Northeastern Atlantic Ocean site. The larger Southern Hemispheric variability compared to the equatorial variability may be caused by transport events, such as a lowered South Pacific Convergence Zone, during different parts of the year. These two sites are the most remote from sources. The low variability of the Equatorial site may also be caused by minimal seasonal variations in photochemical loss rates during the year.

[16] The variability-lifetime relation for the temporal variability case differs from the spatial variability results above. The α values are smaller (0.04–0.14), and the β values are greater (0.84–0.98). In the case of the Southern Pacific Ocean site the relation approaches *Junge*'s [1974] lifetime dependence of $\beta = 1$. This differs from previous results of temporal variability that suggest $\beta \approx 0.5$ [*Gibbs and Slinn*, 1973] but are in the range of *Jaenicke*'s [1982] results. A summary of the spatial and temporal variability-lifetime relation results is shown in Table 2. From the CTM results it can be concluded that both spatial and temporal variability depend crucially on the region or location of sampling.

4. Sources, Sinks, and Variability for a CH_3Br-Like Gas

4.1. Model Simulations

[17] The purpose of these simulations is to examine the variability-lifetime relation dependence on sources (land versus indus-

Table 2. Model Results[a]

α	β	R^2	Species	Location	Description
0.24	0.69	0.99	hydrocarbons	troposphere	land source,
0.17	0.70	0.99	$0.16 < \tau < 7.0$ years	Northern Hemisphere	photochemical loss
0.09	0.81	0.99		Southern Hemisphere	
0.26	0.79	0.99	hydrocarbons	troposphere	land source,
			$0.9 < \tau < 7.0$ years		photochemical loss
0.30	0.57	0.99	hydrocarbons	troposphere	land source,
			$0.44 < \tau < 0.5$ years		photochemical loss
0.04–0.14	0.84–0.98	0.99	hydrocarbons	surface layer, 4 grid	land source,
			$0.2 < \tau < 0.9$ years	locations (ocean)	photochemical loss
0.26	0.77	0.99	CH_3Br-like gas	troposphere	land source,
			$0.8 < \tau < 1.8$		photochemical loss
0.42	0.77	0.99	CH_3Br-like gas	troposphere	industrial source,
			$0.7 < \tau < 1.7$ years		photochemical,
					ocean and soil losses
0.51	0.79	0.99	CH_3Br-like gas	troposphere	industrial source,
			$0.9 < \tau < 2.4$ years		photochemical loss
0.07	0.73	0.97	halocarbons, hydrocarbons	Pacific Ocean subset	PTA model (land
			$0.2 < \tau < 0.9$ years		source, photochemi-
					cal loss), September
0.06	1.30	0.97	C_2H_6, C_2Cl_4, $CHCl_3$,	Pacific Ocean	PTA observations,
			CH_3Cl, CH_3Br		September 1996,
					Colman et al. [1998]
0.23	0.67	0.99	halocarbons, hydrocarbons	Pacific Ocean subset	PTB model (land
			$0.2 < \tau < 0.9$ years		source, photochemi-
					cal loss), March
0.07	1.72	0.97	C_2H_6, C_2Cl_4, $CHCl_3$,	Pacific Ocean	PTB observations,
			CH_3Cl, CH_3Br, CH_2Cl_2		March 1999

[a] Results given in the form $\sigma = \alpha\tau^{-\beta}$. All model results are based on the volume indicated and a time period of 1 year, except the PTA and PTB simulations. PTA and PTB model results are for the month indicated and correspond to the field measurements, which are also shown. Here τ is the global mean steady state lifetime due to tropospheric losses.

trial) and on sinks (photochemical versus photochemical combined with ocean and soil). The variability of a CH_3Br-like gas is measured by the CTM (equation (5)) using the global tropospheric mixing ratios averaged over 1 year. Three scenarios are presented: continental land source combined with photochemical loss, industrial source combined with photochemical loss, and industrial source combined with photochemical, ocean, and soil losses. The tracer source consists of continuous land emissions, weighted either by industrial regions or by continental land area (see section 2). A combination of three distinctly different loss patterns is used, typical for those of CH_3Br: photochemical loss driven by OH concentrations, ocean loss driven by air-sea exchange and chemical loss within the mixed layer, and soil loss driven by a dry deposition velocity (see section 2).

[18] Four simulations using industrial emissions (1.5×10^6 g yr^{-1}) and different k_{OH} loss rates (with no other sinks) are conducted. The preexponential value (A) of k_{OH} is varied, while the exponential factor B remains constant at 1470 K. The same procedure is repeated using photochemical loss plus constant ocean and soil losses. Four different loss rates are used to generate τ ranging from 0.7 to 2.4 years. These simulations represent a baseline for the spatial variability-lifetime relation for CH_3Br-like gases. The procedure is repeated a third time using land emissions and photochemical sink only. This is similar to the simulations in section 3, but the tracer mass and the temperature-dependent OH reaction rate coefficient (B) are specific to CH_3Br, not to CH_3CCl_3.

4.2. Atmospheric Patterns

[19] The 5-day mean, column-integrated losses (in nmol m^{-2} yr^{-1}) for the CH_3Br-like gas with a uniform concentration of 10 pptv are calculated for January and July. The unique seasonality and strength of each loss process (photochemical, ocean, and soil) are shown in Figure 4. When the base-case ($\tau \approx 1$ year) CH_3Br simulation is yearly integrated, the strength of the sinks increases from ocean ($\tau = 4.5$ years) to soil ($\tau = 3.2$ years) to photochemical ($\tau = 2.4$ years).

[20] The latitudinal gradient and mixing ratio values of the CH_3Br-like tracers with $\tau \approx 1$ year are shown in Figure 5 for each of the simulations performed: land source with photochemical loss ($\tau = 0.97$ years), industrial source with photochemical loss ($\tau = 1.00$ year), and industrial source with three losses (photochemical, ocean, and soil ($\tau = 1.05$ years)). The tracer mixing ratios are recorded at the 645-mbar pressure level at two transects, the dateline (180°W) and the prime meridian (0°), during April and September. The Northern Hemispheric mixing ratios are larger and more variable than the Southern Hemispheric values because of the large Northern Hemispheric source in both the industrial and land emissions. The industrial source contributes to a larger latitudinal gradient, as would be expected from the emission patterns shown in Figure 1. The seasonal amplitude (April versus September) is largest for the land-emitted tracer and smallest for the industrial source with three sinks. The dateline transect shows slight differences in mixing ratio compared to the prime meridian transect.

4.3. Variability-Lifetime Analysis

[21] The effect of source and sink patterns on mixing ratio variability is shown in Figure 6a. The variability-lifetime relationships observed here are linear with R^2 values of at least 0.99. The top curve (squares) represents tracers with industrial emissions and photochemical loss, while the bottom curve (circles) represents tracers with continental land emissions and photochemical loss. The industrial source produces more variable trace gas mixing ratios than the uniform continental land source; it also emits a greater fraction at midnorthern latitudes (Figure 1). Other types of source patterns will also be expected to diverge from the variability-lifetime relations derived here. Clearly, the shift in sources produces different variability-lifetime relations, with σ differing by a factor of 2, and inducing an unacceptably large error in the inferred τ. However, the values of β are very similar for both cases (0.79 and 0.77).

[22] The photochemical sink (top curve in Figure 6a) produces much larger σ than the three-component sink (middle curve in Figure 6a). Each case has the same industrial emission pattern,

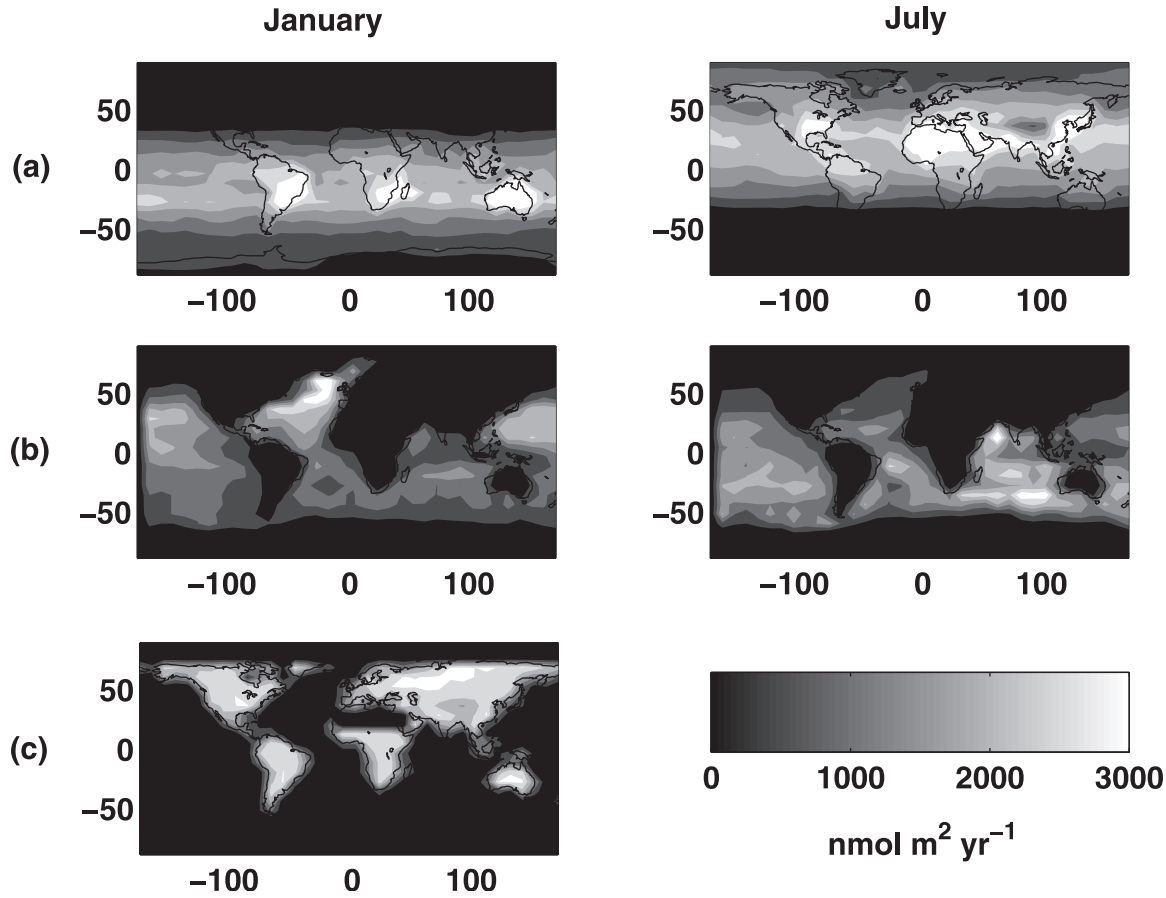

Figure 4. Base-case fluxes for uniform 10-pptv CH_3Br-like gas in the months of January and July in nmol m^{-2} yr^{-1}. (a) Integrated photochemical column loss (b) Ocean uptake (c) Soil uptake. The *y* and *x* axes are latitude and longitude, respectively. Soil uptake does not vary with season. See color version of this figure at back of this issue.

yet, surprisingly, the three-component sink (photochemical, ocean, and soil) dampens the variability. It is probable that the photochemical loss generates the largest σ. This may be because of the large seasonality of the photochemical (OH) sink and the subsequent generation of latitudinal gradients that largely control *s*. Zonal variability in the sink is washed out in a few weeks, but the large interhemispheric gradient is created on seasonal timescales and remains intact. Variability from the ocean loss shifts seasonally as well (on a monthly versus weekly basis), but not as strongly as the photochemical loss, and the land sink is constant with time (Figure 4).

4.4. Loss Patterns and Estimated Error in Variability-Lifetime Analysis

[23] The sensitivity of the variability to various loss types is investigated. This method estimates error associated with using the variability-lifetime analysis to calculate τ of trace gases such as CH_3Br. Simulations are conducted by holding industrial sources and τ constant and scaling each of the three loss terms seven times. One of the baseline results from section 4.3 (industrial source with three losses, τ = 1.05 years) is used for comparison. This base-case simulation includes k_{OH} [*DeMore et al.*, 1997] and ocean loss frequencies for CH_3Br and a generalized soil loss frequency. Together, the three loss frequencies are varied in strength to keep the overall τ close to the CH_3Br base case ($\sum 1/k_i$ = 1.05 year). These simulations are described in Table 3.

[24] The variability-lifetime relation for industrial sources with a mix of photochemical, ocean, and soil loss (middle curve in Figure 6a) represents a base-case scenario for CH_3Br-like gases. In these sensitivity experiments the three sinks are balanced to give a τ of close to one of the base-case examples (τ ≈ 1 year). The balance is achieved by keeping one of the loss frequencies constant to the base-case example while changing the other two loss frequencies by a scaled factor. For example, when the photochemical loss remains constant, then the ocean loss can be increased or decreased and the soil loss can be decreased or increased. These experiments and resulting τ and σ are shown in Tables 3 and 4.

[25] The results of the sensitivity of loss type on σ simulations are plotted as numbered symbols in Figure 6b. There is a small spread in τ, and thus the fitted relation, $\sigma_{trop} = 0.42\tau^{-0.77}$, is used to derive the percent difference in σ as compared with that expected for the base-case example (i.e., the current best guess for the mix of photochemical, ocean, and soil sinks). The largest change in σ from the base case is −18% for variation 7, caused by decreasing the k_{OH} by 50% and increasing the soil deposition velocity by ∼90% (Table 3). The smallest change in σ is +0.5% for variation 5, caused by increasing the k_{OH} by 25% and decreasing the ocean loss frequencies by 50%. The base-case example σ is overestimated by 0.03% using the fitted relation. This is the error associated with the best fit curve (Figure 6b).

[26] When τ is derived from the range of σ observed from the seven results in Table 4, again using the baseline variability-lifetime relation of $\sigma_{trop} = 0.42\tau^{-0.77}$, the resulting τ ranges from 0.79 to 1.26 years, corresponding to a percent error or uncertainty of at least ±21% from the actual τ. This uncertainty factor applies to gases with multiple losses and industrial emissions, such as CH_3Br. This sensitivity study is limited to three loss patterns and seven variations of the strength of each loss. In observations it is likely that there are more variables to be considered, and thus the derived uncertainty should not be considered an upper limit. As

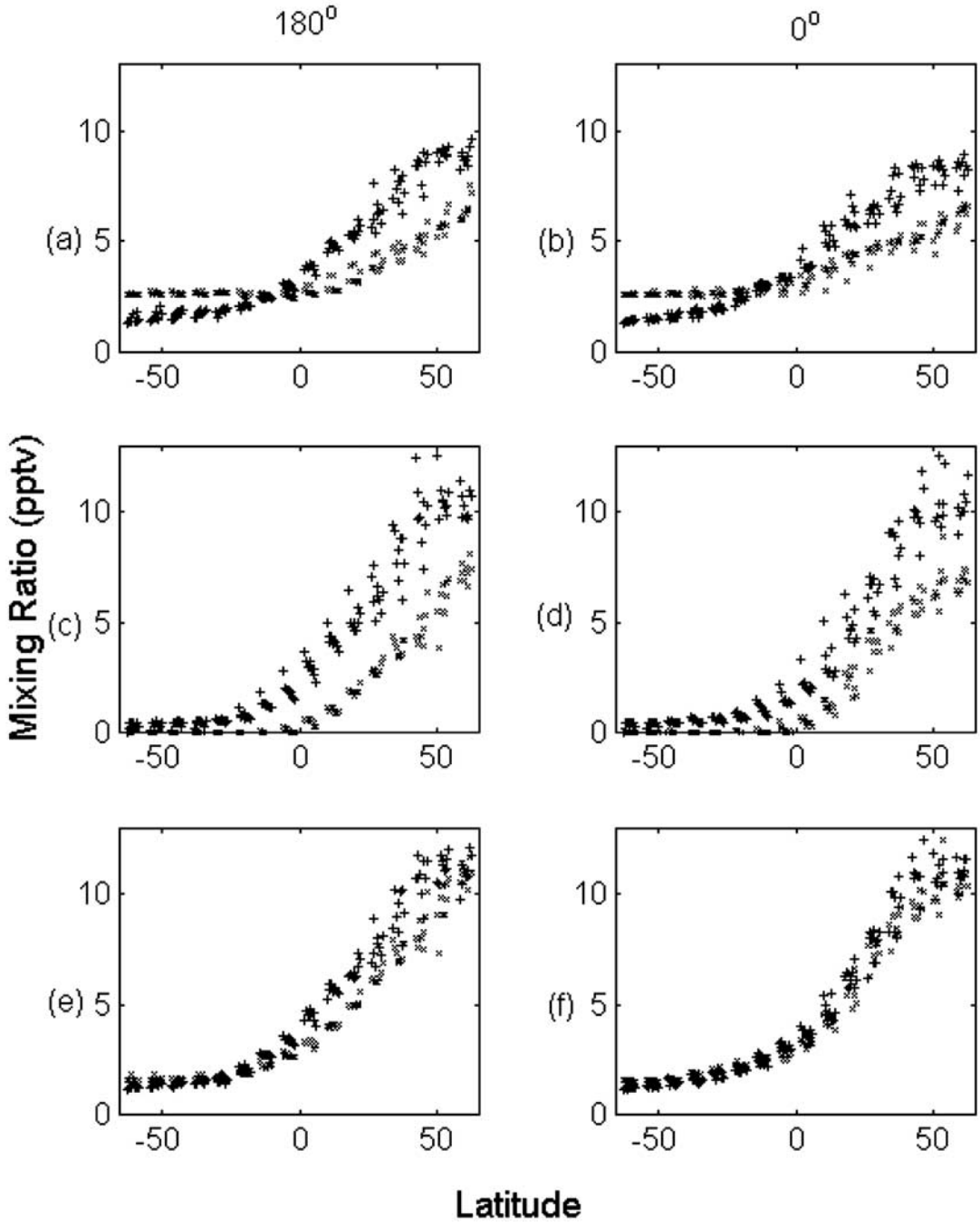

Figure 5. Latitudinal profiles of tracer mixing ratios at the 645-mbar pressure level and at two longitudes (left column: dateline, 180°W; right column: prime meridian, 0°). Pluses represent the month of April and crosses represent the month of September. Nine days of each month are shown, with the latitude slightly offset from the midpoint of the grid for ease in viewing the variability of the mixing ratios. The results of three types of simulations are shown: (a, b) the land-source CH_3Br-like tracer with photochemical loss, (c, d) the industrial-source CH_3Br-like tracer with photochemical loss, and (e, f) the industrial-source CH_3Br-like tracer with three losses (photochemical, ocean, and soil). For each simulation the tracer lifetime is ~1 year.

shown above, sources also will add to this uncertainty, as well as sampling location and timescales.

5. Model Versus PEM-Tropics Observations

5.1. Experimental PTA/PTB

[27] PTA and PTB were NASA airborne campaigns over the Pacific Ocean, aimed at exploring atmospheric chemical composition in this remote, relatively unpolluted region. PTA was conducted from 24 August to 6 October 1996, and PTB was conducted from 6 March to 18 April 1999. Whole air samples were collected in 2-L stainless steel canisters aboard the NASA DC-8 and P-3B aircraft and returned to UCI for subsequent gas chromatographic/mass spectroscopic analysis. *Blake et al.* [2001] describe details of the analysis. Of the many compounds measured in the field, six were chosen for the variability-lifetime analysis ($0.2 < \tau < 1.3$ years): C_2H_6, C_2Cl_4, $CHCl_3$, CH_3Cl, CH_3Br, and CH_2Cl_2, all (except CH_2Cl_2) of which were also used in variability-lifetime analysis

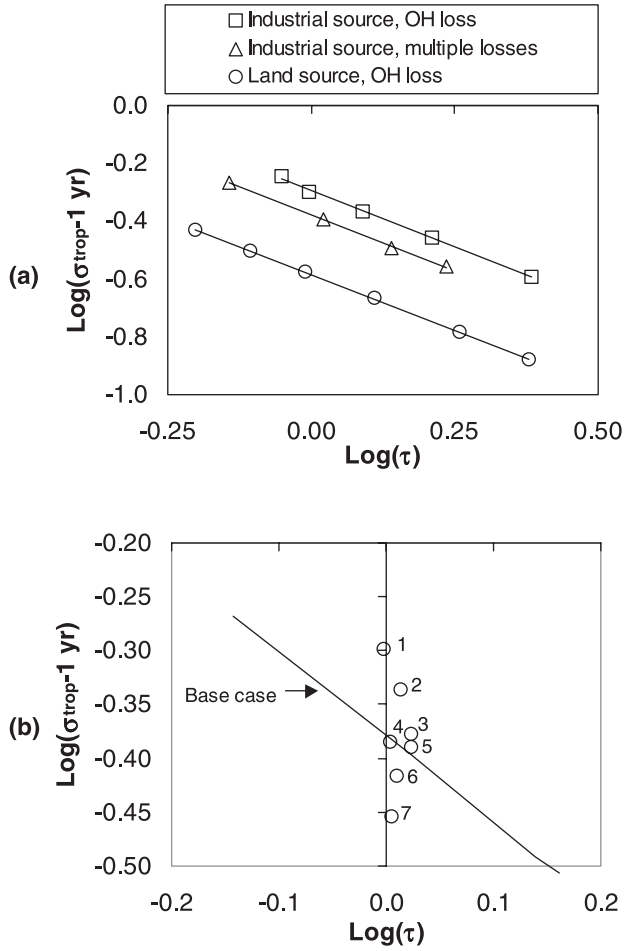

Figure 6. (a) Variability-lifetime results for CH_3Br-like gas. Top and bottom curves show the effect of sources on variability: the land source (circles, $\sigma = 0.26\tau^{-0.77}$) is compared with the industrial source (squares, $\sigma = 0.51\tau^{-0.79}$), both with photochemical loss. Base-case spatial variability-lifetime relation (triangles, $\sigma = 0.42\tau^{-0.77}$) for CH_3Br-like gas with industrial emissions: ocean, soil, and photochemical loss are included, and four different photochemical losses are used to vary the lifetime. $R^2 = 0.99$ for all fitted relations. (b) Base-case (industrial source, multiple losses) variability-lifetime relation from above ($\sigma = 0.42\tau^{-0.77}$) is shown with results (1–7) representing the different variations on losses (see Table 3) on the base case result ($\tau \sim 1$ year). The lifetime was kept fairly constant, and the range in variability is shown. This range in variability demonstrates the uncertainty of using this variability-lifetime relation.

Table 3. Sensitivity Experiments (Loss Types on σ) for CH_3Br-Like Gas[a]

Sink Variation Case	OH Loss	Ocean Uptake	Soil Loss	τ, years
Base				1.05
1[b]	+150%	−100%	−100%	0.99
2	+50%	constant	−60%	1.03
3	constant	+100%	−25%	1.05
4	−18%	+100%	constant	1.05
5	+25%	−50%	constant	1.01
6	constant	−50%	+32%	1.02
7	−50%	constant	+88%	1.01

[a] Photochemical (OH) loss representing the change in rate constant, k_{OH}. Ocean uptake represents the change in the ocean loss frequency, which combines air/sea exchange, mixing, and chemical loss. Soil loss represent the change in land-weighted deposition velocity. The base-case fluxes foe January and July are shown in Figure 4.

[b] Part of the top curve that includes only photochemical loss.

by *Colman et al.* [1998]. The gas chromatographic procedure used in PTA was unable to separate CH_2Cl_2 from methyl nitrate, so CH_2Cl_2 was not quantified in the first experiment. Improvements of the separation techniques enabled this measurement for PTB. The measured gases were selected from others because of their non-proximity to sources, and the analytical precision was less than their measured σ. For the variability-lifetime analysis, 3936 and 4504 samples are used from PTA and PTB, respectively. *Colman et al.* [1998] and *Blake et al*. [2000] show the spatial distribution of samples collected in PTA and PTB, respectively.

5.2. Model Simulation

[28] Tracers with a continental land source (section 2) and τ ranging from 0.2 to 0.9 years (with respect to photochemical loss) are used in the CTM to simulate compounds analyzed during the Global Tropospheric Experiments PTA and PTB. Areas from 32°S to 0°, 168°E to 152°W, and 0° to 32°N, 173°W to 133°W are monitored in the CTM to simulate the regions sampled during the PTA and PTB (Figure 2a). All seven layers of the troposphere are included in the CTM analysis of σ (equation (5)). The monthly averaged σ for March and September are calculated (σ_{PT}). These months are chosen to coincide with the sampling times of PTA and PTB, September 1996 and March 1999, respectively. The variability-lifetime relation was derived previously in the PTA data set and used to estimate τ of CH_3Br as 0.8 ± 0.1 year [*Colman et al.*, 1998]. Here both the PTA and PTB data sets are used to examine seasonal or other dependencies of σ. The modeled tracers are designed to fall in the same range of photochemical (OH) reactivity as the compounds above. The variability of the PTA and PTB data is calculated from all available mixing ratio measurements as a whole and also in latitude/longitude groupings that resemble the model resolution for comparison.

5.3. Results and Discussion

[29] The results of the variability-lifetime analysis for PTA and PTB are shown in Figure 7. The variability observed in PTB is greater than in PTA for both the model and observations. The modeled results resemble the results from section 3, with an average of the two seasonal β of 0.70, compared to β of 0.69 from the global troposphere (Figure 3a). Although the β values largely differ between the model (0.67–0.73) and observations (1.30–1.72), there are some similarities in the variability-lifetime behavior of the modeled and experimental results. Within the model, there is a seasonal dependence on σ, and this may also be

Table 4. Effect of Loss Types and Weightings on σ[a]

Sink Variation	τ, years	σ_{trop}	$\Delta\sigma_{trop}$, percent	Δτ, percent
Base Case	1.05	0.402	+0.03	−0.04
1[b]	0.99	0.504	+16.6	−21.0
2	1.03	0.461	+11.4	−14.6
3	1.05	0.419	+4.3	−5.5
4	1.05	0.407	+1.5.	−1.9
5	1.01	0.413	+0.5	−0.6
6	1.02	0.384	−7.2	+9.4
7	1.01	0.352	−17.8	+23.8

[a] The $\Delta\sigma_{trop}$ is calculated from the difference between the modeled σ_{trop} and the baseline fit ($\sigma = 0.42\tau^{-0.77}$) using the values of τ shown. The corresponding percent Δ τ is also shown.

[b] Part of the top curve that includes only photochemical loss.

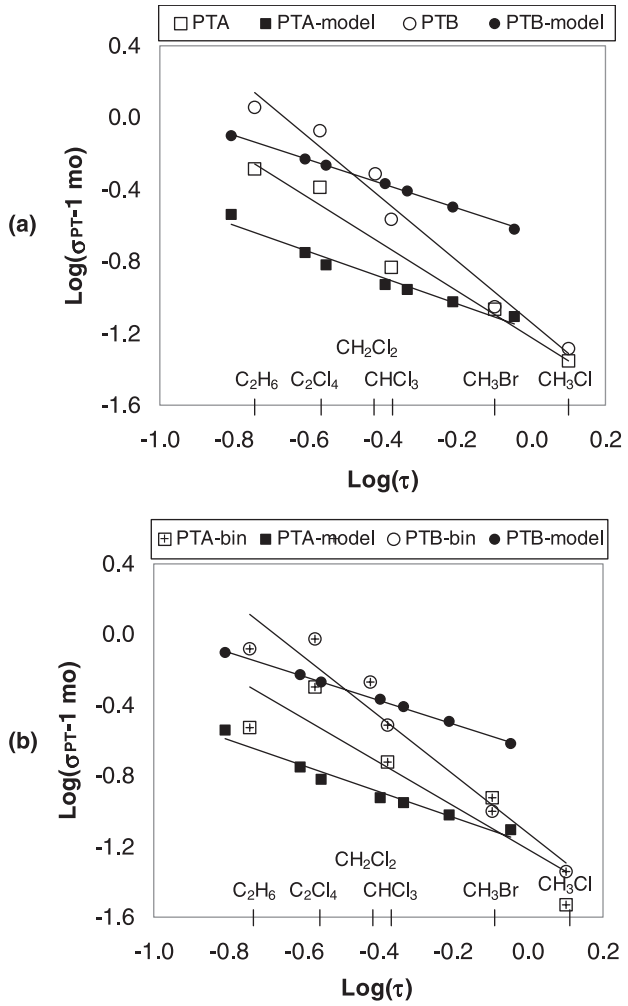

Figure 7. (a) Model versus observed spatial variability for PEM-Tropics A (September, squares) and PEM-Tropics B (March, circles). Open symbols represent field observations over the whole sampling area of PTA ($\sigma = 0.06\tau^{-1.30}$, $R^2 = 0.97$) and PTB ($\sigma = 0.07\tau^{-1.72}$, $R^2 = 0.97$), while solid markers represent model results over the subset region of the Pacific Ocean shown in Figure 2a ($\sigma = 0.07\tau^{-0.73}$, $R^2 = 0.97$ for September and $\sigma = 0.23\tau^{-0.67}$, $R^2 = 0.99$ for March). (b) Model results from Figure 7a shown with PTA and PTB mixing ratios averaged in 8° × 10° latitude/longitude boxes resembling the CTM resolution. Power relationships resulting from the binned observations are $\sigma = 0.06\tau^{-1.23}$ ($R^2 = 0.81$) for PTA and $\sigma = 0.08\tau^{-1.66}$ ($R^2 = 0.94$) for PTB.

true for PTA and PTB gases (except perhaps the methyl halides, which show little difference in σ). PTA was conducted during the southern tropical dry season, while PTB was conducted during the southern tropical wet season. The seasonal differences in the photochemical loss rates can explain the values of σ differing by about a factor of 2.

[30] Each experiment encountered different types of air masses; for example, PTB was influenced by minimally polluted Northern Hemispheric air masses, while PTA was influenced by biomass burning from Southern Hemispheric regions [*Blake et al.*, 2001]. Thus the observations may reflect not just a seasonal dependence, but also a chemical signature resulting from the type of air masses encountered (e.g., pollution episodes). From the source/sink analysis in section 4.3 (see Figure 6a), the difference between the observed and modeled data could be caused by the different sources and sinks of those gases measured in the field. The observed PTA/PTB relationship can probably be better understood in terms of two classes of gases: one with higher σ (C_2Cl_4, C_2H_6, and CH_2Cl_2) coming predominantly from industrial sources and the other with lower σ (CH_3Br and CH_3Cl) coming predominantly from natural or ocean sources.

[31] Another possible explanation of the disagreement of the model and observations is the volume or locations of averaging. PTA sampled more frequently in the Southern Hemisphere than PTB. The model averaging volume (Figure 2a) remains the same in both simulations. To determine if this is affecting the variability, the PTA and PTB mixing ratios are divided into 8° × 10° latitude/longitude boxes with the same vertical resolution as the CTM. These values are then averaged, and σ is calculated (Figure 7b). The binned results, however, do not change much from the ungrouped results in Figure 7a. The fitted relationships are much weaker, with R^2 values of 0.81 and 0.94 for PTA and PTB, respectively. The values of β are still >1 and show a different behavior from the modeled results (Figure 7b).

[32] The model simulations cannot accurately reproduce the observations from PTA and PTB. The model did not attempt to replicate the biomass burning or pollution events encountered in PTA and PTB. The results from sections 3 and 4 indicate that the variability-lifetime relation depends largely on the sampling area and time frame and also on the sources and sinks of the gases in question. The analytical precision of the mixing ratio measurements (1–3%) is able to resolve the measured σ of the compounds in Figure 7. Uncertainties in the τ estimates for the measured PTA and PTB gases may be high, but even a 30% change in τ of the four or five gases results in a 15% change in τ of CH_3Br [*Colman et al.*, 1998]. The σ values for CH_3Br did not change much from PTA to PTB, which is why using the fitted variability-lifetime relations leads to a similar value of τ (0.8 ± 0.1 years). The uncertainty derived from section 4.4 only broadens this range slightly (0.8 ± 0.15 years). However, when considering a gas with larger σ, using the fitted relationships (Figure 7) to derive a τ will give inconsistent results. For example, the fitted PTA relationship will yield a τ of 0.2 years for a gas with a measured σ of 0.5, while the fitted PTB relationship will yield a τ of 0.3 years. This is a 50% difference in derived τ. Therefore variability-lifetime analysis is not an accurate method of determining the τ of tropospheric gases in general. No consistent relation could be derived from the 3-D model or from the PTA and PTB data set.

[33] There are some uncertainties and assumptions in using the model that could be considered. The model assumes that all gases have the same source patterns (either industrial or continental land) and that the only chemical loss is due to reaction with OH. Uncertainty lies within the k_{OH} values used from *DeMore et al.* [1997] and also in the OH concentrations (they are not varied interannually). The model resolution could also be biasing the results. Higher spatial resolution could increase or decrease the values of σ.

6. Conclusions

[34] From the 3-D model results it can be concluded that the systematically different variability-lifetime relationships for different source/sink patterns and spatial /temporal sampling patterns make empirical calibration using a variety of different trace gases unreliable. For example, in the case of a CH_3Br-like gas with τ of ~1 year, rescaling the sinks between photochemistry, ocean, and soil changes the σ by up to ±17%. Such differences cause a ±20% uncertainty due to the sink pattern alone when σ is used to derive τ. The variability-lifetime relation depends greatly on the location of sampling or averaging (Globe, Northern and Southern Hemispheres, or Pacific Ocean), the time period of averaging (monthly or yearly), and the types of sources (industrial or land based) and sinks (photochemical, ocean, or soil) of the trace gases. The modeling results here give α values of 0.04–0.51 and ß values

of 0.57–0.98. These compare to *Hamrud*'s [1983] 2-D modeling study results of α (0.04–0.49) and β (0.63–0.91). The observed variability-lifetime dependence in the PTA and PTB data was unable to be reproduced by the model. The CH_3Br τ estimated from these observations was, however, consistent (0.8 years). If no other estimate is available for τ of a gas, using variability-lifetime analysis could give a range of expected values. The variability-lifetime relation is not universal or unique and should be used only to compare consistent data sets for gases with similar source and sink patterns.

Notation

A preexponential factor of rate constant k, in cm^3 $molecules^{-1}$.
B exponential term of rate constant k, in inverse temperature units, K^{-1}.
k second-order rate constant, in cm^3 $molecules^{-1}$ s^{-1}.
L integrated tropospheric loss, in kg yr^{-1}.
M global mass content, in kilograms.
s standard deviation, in pptv.
s_w area-weighted standard deviation, in pptv.
x_i mixing ratio, in pptv.
$\bar{x}$ mean mixing ratio, in pptv.
$\bar{x}_w$ area-weighted mean mixing ratio, in pptv.
w area of model grid box, in square meters.
α variability-lifetime relation constant.
β variability-lifetime relation power term.
σ relative standard deviation.
τ global mean state tropospheric lifetime, in years.

[35] **Acknowledgments.** The authors would like to thank all those who have participated in the PEM-Tropics campaign, especially the following members of the Rowland/Blake Laboratory at UCI: Nicola Blake, Isobel Simpson, Jimena Lopez, Oliver Wingenter, Barkley Sive, Murray McEachern, John Bilicska, Aaron Swanson, Aaron Katzenstein, Simone Meinardi, Brent Love, Kevin Gervais, Jason Paisley, Jennifer Lapierre, Adam Hill, Nina Riga, and Barbara Yu. PEM-Tropics A and B were funded by NASA grants NAG-1-1777 and NCC-1-299.

References

Balkanski, Y. J., and D. J. Jacob, Transport of continental air to the subantarctic Indian Ocean, *Tellus, Ser. B*, *42*, 62–75, 1990.

Balkanski, Y. J., D. J. Jacob, G. M. Gardner, W. C. Graustein, and K. K. Turekian, Transport and residence times of tropospheric aerosols inferred from a global three-dimensional simulation of 210Pb, *J. Geophys. Res.*, *98*, 32,627–32,644, 1993.

Blake, N. J., et al., Large-scale latitudinal and vertical distributions of NMHCs and selected halocarbons in the troposphere over the Pacific Ocean during the March-April 1999 Pacific Exploratory Mission (PEM-Tropics B), *J. Geophys. Res.*, *106*, 10.1029/2000JD900773, 2001.

Colman, J. J., D. R. Blake, and F. S. Rowland, Atmospheric residence time of CH_3Br estimated from the Junge spatial variability relation, *Science*, *281*, 392–396, 1998.

DeMore, W. B., S. P. Sander, D. M. Golden, R. F. Hampson, M. J. Kurylo, C. J. Howard, A. R. Ravishankara, C. E. Kolb, and M. J. Molina, Chemical kinetics and photochemical data for use in stratospheric modeling, *Publ. 97-4/12*, Jet Propul. Lab., Calif. Inst. of Technol., Pasadena, 1997.

Ehhalt, D. H., F. Rohrer, A. Wahner, M. J. Prather, and D. R. Blake, On the use of hydrocarbons for the determination of tropospheric OH concentrations, *J. Geophys. Res.*, *103*, 18,981–18,997, 1998.

Fung, I., C. J. Tucker, and K. C. Prentice, Application of AVHRR vegetation index to study atmosphere-biosphere exchange of CO_2, *J. Geophys. Res.*, *92*, 2999–3016, 1987.

Fung, I., J. John, J. Lerner, E. Matthews, M. Prather, L. P. Steele, and P. J. Fraser, Three-dimensional model synthesis of the global methane cycle, *J. Geophys. Res.*, *96*, 13,033–13,065, 1991.

Gibbs, A. G., and W. G. N. Slinn, Fluctuations in trace gas concentrations in the troposphere, *J. Geophys. Res.*, *78*, 574–576, 1973.

Hamrud, M., Residence time and spatial variability for gases in the atmosphere, *Tellus, Ser. B*, *35*, 295–303, 1983.

Hansen, J., G. Russell, D. Rind, P. Stone, A. Lacis, S. Lebedeff, R. Ruedy, and L. Travis, Efficient three-dimensional global models for climate studies, Models I and II, *Mon. Weather Rev.*, *111*, 609–662, 1983.

Jacob, D. J., and M. J. Prather, Radon-222 as a test of the boundary-layer convection in a general circulation model, *Tellus, Ser. B*, *42*, 118–134, 1990.

Jacob, D. J., M. J. Prather, S. C. Wofsy, and M. B. McElroy, Atmospheric distribution of ^{85}Kr simulated with a general circulation model, *J. Geophys. Res.*, *92*, 6614–6626, 1987.

Jacob, D. J., et al., Simulation of summertime ozone over North America, *J. Geophys. Res.*, *98*, 14,797–14,816, 1993a.

Jacob, D. J., J. A. Logan, G. M. Gardner, R. M. Yevich, C. M. Spivakovsky, S. C. Wofsy, J. M. Munger, S. Sillman, and M. J. Prather, Factors regulating ozone over the United States and its export to the global atmosphere, *J. Geophys. Res.*, *98*, 14,817–14,826, 1993b.

Jaenicke, R., Physical aspects of the atmospheric aerosol, in *Chemistry of the Unpolluted Troposphere*, edited by H. W. Georgii and W. Jaeschke, pp. 341–373, D. Reidel, Norwell, Mass., 1982.

Jobson, B. T., D. D. Parrish, P. Goldan, W. Kuster, F. C. Fehsenfeld, D. R. Blake, N. J. Blake, and H. Niki, Spatial and temporal variability of nonmethane hydrocarbon mixing ratios and their relation to photochemical lifetime, *J. Geophys. Res.*, *103*, 13,557–13,567, 1998.

Jobson, B. T., S. A. McKeen, D. D. Parrish, F. C. Fehsenfeld, D. R. Blake, A. H. Goldstein, S. M. Schauffler, and J. W. Elkins, Trace gas mixing ratio variability versus lifetime in the troposphere and stratosphere: Observations, *J. Geophys. Res.*, *104*,16,091–16,113, 1999.

Junge, C. E., *Air Chemistry and Radioactivity*, Academic, San Diego, Calif., 1963.

Junge, C. E., Residence time and variability of tropospheric trace gases, *Tellus*, *4*, 477–488, 1974.

Olsen, S. C., B. J. Hannegan, X. Zhu, and M. J. Prather, Evaluating ozone depletion from very short lived halocarbons, *Geophys. Res. Lett.*, *27*, 1475–1478, 2000.

Prather, M., and C. M. Spivakovsky, Tropospheric OH and the lifetimes of hydrochlorofluorocarbons, *J. Geophys. Res.*, *95*, 18,723–18,729, 1990.

Prather, M., M. McElroy, S. Wofsy, G. Russell, and D. Rind, Chemistry of the global troposphere: Fluorocarbons as tracers of air motion, *J. Geophys. Res.*, *92*, 6579–6613, 1987.

Prinn, R. G., R. F. Weiss, B. R. Miller, and J. Huang, Atmospheric trends and lifetime of CH_3CCl_3 and global OH concentrations, *Science*, *269*, 187–192, 1995.

Slinn, W. G. N., A simple model for Junge's relationship between concentration fluctuations and residence times for tropospheric trace gases, *Tellus, Ser. B*, *40*, 229–232, 1988.

Spivakovsky, C. M., R. Yevich, J. A. Logan, S. C. Wofsy, M. B. McElroy, and M. J. Prather, Tropospheric OH in a three-dimensional chemical tracer model: An assessment based on observations of CH_3CCl_3, *J. Geophys. Res.*, *95*, 18,441–18,471, 1990.

Williams, J., et al., Variability-lifetime relationship for organic trace gases: A novel aid to compound identification and estimation of HO concentrations, *J. Geophys. Res.*, *105*, 20,473–20,486, 2000.

Yvon, S. A., and J. H. Butler, An improved estimate of the oceanic lifetime of atmospheric CH_3Br, *Geophys. Res. Lett.*, *23*, 53–56, 1996.

D. R. Blake, N. A. C. Johnston, and F. S. Rowland, Department of Chemistry, University of California, Irvine, 516 Rowland Hall, Irvine, CA 92697-2025, USA. (drblake@uci.edu; najohnston@lcsc.edu; rowland@uci.edu)

J. J. Colman, Los Alamos National Laboratory, Los Alamos, NM 87545, USA. (jonah@kokopelli.lanl.gov)

M. J. Prather, Department of Earth Systems Science, University of California, Irvine, Irvine, CA 92697-3100, USA. (mprather@uci.edu)

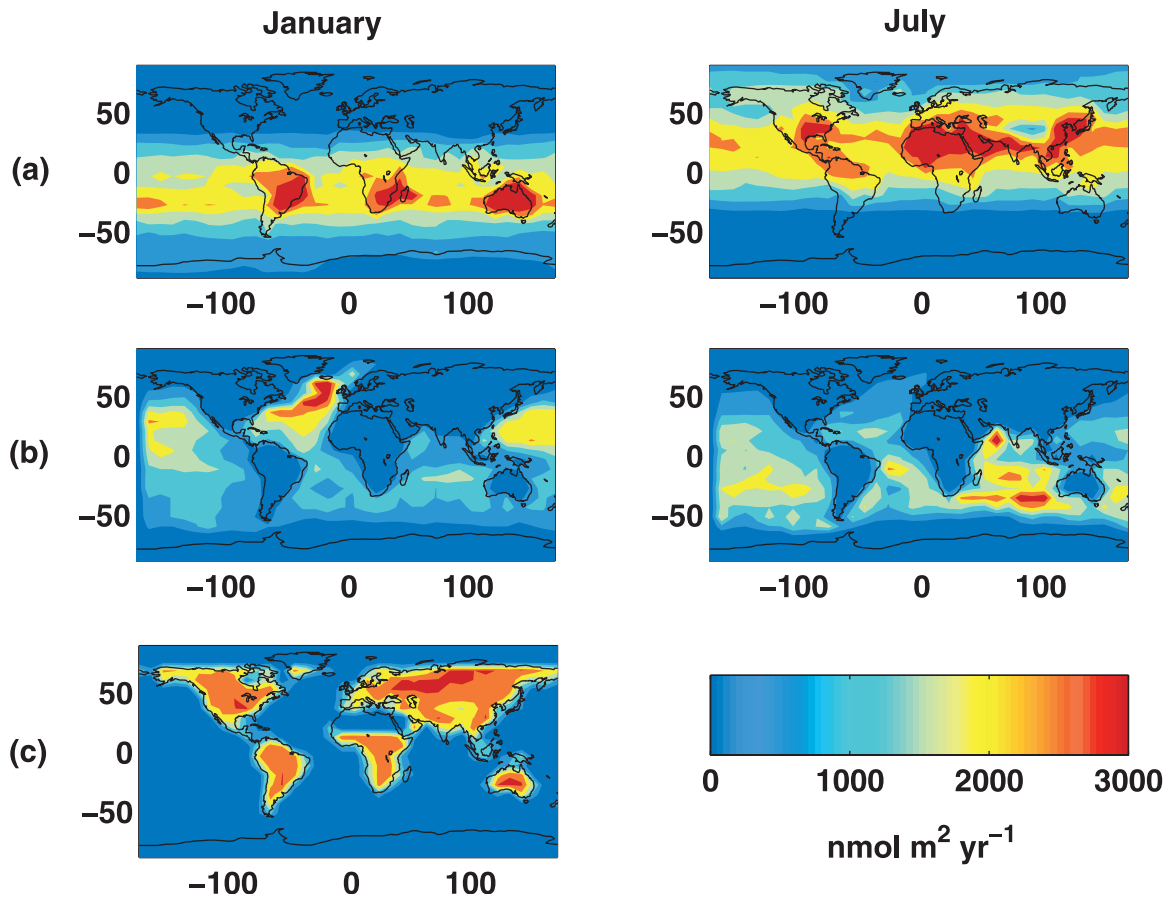

Figure 4. Base-case fluxes for uniform 10-pptv CH_3Br-like gas in the months of January and July in nmol m^{-2} yr^{-1}. (a) Integrated photochemical column loss (b) Ocean uptake (c) Soil uptake. The *y* and *x* axes are latitude and longitude, respectively. Soil uptake does not vary with season.